Redshift drift in a universe with structure: Lemaître-Tolman-Bondi structures with arbitrary angle of entry of light

Sofie Marie Koksbang[1,*] and Asta Heinesen[2,†]

[1]*CP*^{3}*-Origins, University of Southern Denmark, Campusvej 55, DK-5230 Odense M, Denmark*
[2]*Univ Lyon, Ens de Lyon, Univ Lyon1, CNRS, Centre de Recherche Astrophysique de Lyon UMR5574, F–69007, Lyon, France*

(Received 24 May 2022; accepted 15 June 2022; published 1 August 2022)

We consider the redshift drift and position drift associated with astrophysical sources in a formalism that is suitable for describing emitters and observers of light in an arbitrary spacetime geometry, while identifying emitters of a given null-geodesic bundle that arrives at the observer worldline. We then restrict the situation to the special case of a Lemaître-Tolman-Bondi (LTB) geometrical structure and solve for light rays propagating through the structure with arbitrary impact parameters, i.e., with arbitrary angles of entry into the LTB structure. The redshift drift signal emitted by comoving sources and viewed by a comoving observer turns out to be dominated by Ricci curvature and electric Weyl curvature contributions as integrated along the connecting light ray. This property simplifies the computations of the redshift drift signal tremendously, and we expect that the property extends to more complicated models including Swiss-cheese models. When considering several null rays with random impact parameters, the mean redshift drift signal is well approximated by a single Ricci focusing term. This suggests that the measurement of cosmological redshift drift can be used as a direct probe of the strong energy condition in a realistic universe where photons pass through many successive structures.

DOI: 10.1103/PhysRevD.106.043501

I. INTRODUCTION

Redshift drift is the temporal change in redshift of light arriving from a distant source as viewed by the observer [1,2]. The detection of redshift drift is a cornerstone of upcoming precise cosmological measurements [3] and makes possible the direct determination of kinematic properties of the Universe, which would otherwise rely on indirect inference and the assumption of a cosmological model. Redshift drift is a probe of dark energy within the Friedmann-Lemaître-Robertson-Walker (FLRW) universe models [4,5], but it might be used as a probe of violation of the strong energy condition within much broader universe geometries [6,7]. Redshift drift might also be used as a test of the FLRW spacetime conjecture [8,9].

The redshift drift signal has mostly been analyzed within the FLRW universe models, but analytical and numerical investigations have also been carried out within Stephani, Lemaître-Tolman-Bondi (LTB), Bianchi I, and Szekeres models [7,10–18]. Convenient representations of redshift drift within arbitrary spacetime geometries have recently been formulated [8,19], and a promising numerical tool for fast computation of drift effects for a given specified metric description has been proposed [20,21].

The redshift drift representation for an arbitrary geometrical setting as formulated in Ref. [8] is useful for analyzing potential systematic departures from the FLRW redshift drift prediction induced by local structures [8], for independent observational tests of the strong energy condition [6], and for performing model-independent cosmographic analyses of data [22]. The representation is furthermore useful for investigating individual curvature and kinematic contributions to the final redshift drift signal within model universes of interest.

In this paper, we consider the redshift drift in a class of LTB models with light propagating through the structure with arbitrary angles of entry. The investigated LTB model profile describes a central underdensity surrounded by a steep overdensity and thus might be used as a crude model of a void with surrounding filaments of galaxies. Using the framework developed in Refs. [6,8,22] to decompose the redshift drift signal allows us to analyze the hierarchy of multipole terms contributing to the signal along the light beam, when the light passes through the LTB structure. We analyze the relative magnitudes of the individual terms as well as cancellation effects related to these terms; in particular, we analyze the conjecture that Ricci focusing dominates the redshift drift signal when light rays are

*koksbang@cp3.sdu.dk
†asta.heinesen@ens–lyon.fr

traversing many structures by considering the situation where many light rays traverse a single structure with different (random) impact parameters.

In Sec. II we review the general expression for the redshift drift signal in terms of the physically interpretable multipole decomposition and consider the multipole coefficients in the special case of an LTB spacetime. In Sec. III we describe the details of our analysis regarding the LTB model parametrization and light propagation. In Sec. IV we describe the results of our analysis, and we conclude in Sec. V.

Notation and conventions: Units are used in which $c = 1$. Greek letters $\mu, \nu, \ldots$ label spacetime indices in a general basis while Latin letters $i, j, \ldots$ denote spatial indices relative to a specified foliation frame. Einstein notation is used such that repeated indices are summed over. The signature of the spacetime metric $g_{\mu\nu}$ is $(-+++)$, and the connection ∇_μ is the Levi-Civita connection. Round brackets () containing indices denote symmetrization in the involved indices, and square brackets [] denote antisymmetrization. Bold notation $\boldsymbol{V}$ for the basis-free representation of vectors V^μ is used occasionally. A subscripted comma followed by an index indicates a partial derivative.

II. MULTIPOLE DECOMPOSITION OF THE REDSHIFT DRIFT SIGNAL

In this section we consider the multipole decomposition of the redshift drift signal developed in Refs. [6,8,22], which is appropriate for analyzing kinematic and curvature contributions to the drift of the redshift of a source. In Sec. II A we consider the decomposition in a general spacetime setting with an arbitrary observer congruence, and we then move on to analyze the special case of an LTB metric with comoving observers in Sec. II B.

A. General spacetime

Following [6,8,22] we consider a general congruence of emitters and observers (denoted the "observer congruence") in an arbitrary spacetime. We let the observer congruence be generated by the 4-velocity field $\boldsymbol{u}$ and parametrized by the proper time function τ satisfying $\dot{\tau} = 1$, where $\dot{} \equiv u^\mu \nabla_\mu$ is the directional derivative along the observer congruence flow lines. The general kinematic decomposition associated with the frame of the observer congruence is

$$\begin{aligned} \nabla_\nu u_\mu &= \frac{1}{3}\theta h_{\mu\nu} + \sigma_{\mu\nu} + \omega_{\mu\nu} - u_\nu a_\mu, \\ \theta &\equiv \nabla_\mu u^\mu, \qquad \sigma_{\mu\nu} \equiv h^\beta_{\langle\nu} h^\alpha_{\mu\rangle} \nabla_\beta u_\alpha, \\ \omega_{\mu\nu} &\equiv h^\beta_\nu h^\alpha_\mu \nabla_{[\beta} u_{\alpha]}, \qquad a^\mu \equiv \dot{u}^\mu, \end{aligned} \tag{1}$$

where $h_\mu{}^\nu \equiv u_\mu u^\nu + g_\mu{}^\nu$ is the spatial projection tensor relative to the observer congruence and where $\langle\rangle$ is the traceless and symmetric part of a spatially projected tensor.[1]

We may consider two causally connected members of the observer congruence with worldlines γ_o and γ_e passing through the events of observation $\mathcal{O}$ and emission $\mathcal{E}$ of a null geodesic ray. Let $\boldsymbol{k}$ be the 4-momentum of a 4-dimensional noncaustic geodesic null congruence that contains this null ray and which creates a bijection between γ_o and γ_e in a neighborhood around the points $\mathcal{O}$ and $\mathcal{E}$. We define the photon energy as measured by members of the observer congruence $E \equiv -u^\mu k_\mu$, and the spatial unit vector $e^\mu \equiv u^\mu - \frac{1}{E}k^\mu$ describing the direction of observation or the "viewing angle" of the light ray as seen by the same observers. We introduce the drift of the viewing angle

$$\kappa^\mu \equiv h^\mu{}_\nu \dot{e}^\nu, \tag{2}$$

which describes the change of spatial direction of incoming light as seen in the observer congruence reference frame. When (2) is evaluated at $\mathcal{O}$, it represents the position drift of the astrophysical emitter as viewed on the observer's sky.

The drift of the redshift, $z \equiv E_{\gamma_e}/E_{\gamma_o} - 1$, as observed by the observer along γ_o in the vicinity of $\mathcal{O}$, can be written as the integral

$$\left.\frac{dz}{d\tau}\right|_{\mathcal{O}} = E_\mathcal{E} \int_{\lambda_\mathcal{E}}^{\lambda_\mathcal{O}} d\lambda\, \Pi, \qquad z \equiv \frac{E_\mathcal{E}}{E_\mathcal{O}} - 1 \tag{3}$$

where λ is an affine parameter along the null geodesic congruence satisfying $k^\mu \nabla_\mu \lambda = 1$. Using the traceless multipole decomposition in $\boldsymbol{e}$ and $\boldsymbol{\kappa}$, the integrand Π can be written as [22]

$$\Pi = -\kappa^\mu \kappa_\mu + \Sigma^o + e^\mu \Sigma^{\boldsymbol{e}}_\mu + e^\mu e^\nu \Sigma^{\boldsymbol{ee}}_{\mu\nu} + e^\mu \kappa^\nu \Sigma^{\boldsymbol{e\kappa}}_{\mu\nu} \tag{4}$$

with coefficients

$$\begin{aligned} \Sigma^o &\equiv -\frac{1}{3}u^\mu u^\nu R_{\mu\nu} + \frac{1}{3}D_\mu a^\mu + \frac{1}{3}a^\mu a_\mu, \\ \Sigma^{\boldsymbol{e}}_\mu &\equiv -\frac{1}{3}\theta a_\mu - a^\nu \sigma_{\mu\nu} + 3a^\nu \omega_{\mu\nu} - h^\nu_\mu \dot{a}_\nu, \\ \Sigma^{\boldsymbol{ee}}_{\mu\nu} &\equiv a_{\langle\mu} a_{\nu\rangle} + D_{\langle\mu} a_{\nu\rangle} - u^\rho u^\sigma C_{\rho\mu\sigma\nu} - \frac{1}{2}h^\alpha_{\langle\mu} h^\beta_{\nu\rangle} R_{\alpha\beta}, \\ \Sigma^{\boldsymbol{e\kappa}}_{\mu\nu} &\equiv 2(\sigma_{\mu\nu} - \omega_{\mu\nu}), \end{aligned} \tag{5}$$

where $R_{\mu\nu}$ is the Ricci curvature tensor, and $C_{\rho\mu\sigma\nu}$ is the Weyl curvature tensor. The operator D_μ is the spatial covariant derivative, which is defined through its action

[1] See [23] for details on the unique traceless decomposition of spatial symmetric tensors, and see [24] for the explicit decomposition for tensors with up to six indices.

on an arbitrary tensor field: $D_\mu T_{\nu_1,\ldots,\nu_n}{}^{\gamma_1,\ldots,\gamma_m} \equiv h^{\alpha_1}_{\nu_1}\ldots h^{\alpha_n}_{\nu_n} h^{\gamma_1}_{\beta_1}\ldots h^{\gamma_m}_{\beta_m} h^{\sigma}_{\mu} \nabla_\sigma T_{\alpha_1,\ldots,\alpha_n}{}^{\beta_1,\ldots,\beta_m}$.

Regarding the decomposition in (4), we note that the truncation of the multipole series at second order in the direction variables $\boldsymbol{e}$ and $\boldsymbol{\kappa}$ of the photon congruence is *exact* for any spacetime description. The coefficients of the series are constructed from the kinematic variables of the observer congruence together with the Ricci focusing term $u^\mu u^\nu R_{\mu\nu}$ and the electric part of the Weyl tensor $u^\rho u^\sigma C_{\rho\mu\sigma\nu}$.

B. Lemaître-Tolman-Bondi spacetime

We now consider the special case of the spherically symmetric LTB spacetime metric [25–27] (see, e.g., the books [28,29] for an introduction). We write the LTB line element in spherical coordinates $x^\mu = (t, r, \theta, \phi)$ adapted to the center of the LTB structure as

$$\mathrm{d}s^2 = -\mathrm{d}t^2 + R(t,r)\mathrm{d}r^2 + A^2(t,r)(\mathrm{d}\theta^2 + \sin^2(\theta)\mathrm{d}\phi^2), \quad (6)$$

with $R(t,r) \equiv (\partial_r A(t,r))^2/(1-k(r))$, where $k(r)$ specifies the spatial Ricci curvature of the LTB model [30] and reduces to a constant times r^2 in the FLRW spacetime limit. The metric is required to be a solution to the Einstein equation $R_{\mu\nu} - R g_{\mu\nu}/2 = 8\pi G T_{\mu\nu}$ with a dust source, such that the energy momentum tensor reads $T_{\mu\nu} = \rho \delta^t_\mu \delta^t_\nu$; for the explicit form of the independent components of Einstein's equations, see Sec. III A where we also specify the LTB solution used in our analysis. We consider an observer congruence that is comoving with the foliation of the metric representation in (6), such that $u^\mu = \delta^\mu_t$. It follows immediately that $\omega_{\mu\nu} = 0$ and $a^\mu = 0$ in the kinematic decomposition (1), and the multipole coefficients in (5) read

$$\Sigma^o = -\frac{1}{3} u^\mu u^\nu R_{\mu\nu}, \qquad \Sigma^{\boldsymbol{e}}_\mu = 0,$$
$$\Sigma^{\boldsymbol{ee}}_{\mu\nu} = -u^\rho u^\sigma C_{\rho\mu\sigma\nu}, \qquad \Sigma^{\boldsymbol{e\kappa}}_{\mu\nu} = 2\sigma_{\mu\nu} \quad \text{(LTB)}, \quad (7)$$

which can be straightforwardly computed in terms of the LTB metric components (6) and their gradients. We list the multipole terms for the LTB metric in Appendix A for convenience.

In the case of a radially propagating congruence of photons, $\boldsymbol{\kappa}$ vanishes, and the redshift drift signal is determined solely from Ricci focusing and electric Weyl curvature. In general, however, the propagation of photons with a nonzero impact parameter relative to the LTB structure will give rise to the additional terms $-\kappa^\mu \kappa_\mu$ and $e^\mu \kappa^\nu \Sigma^{\boldsymbol{e\kappa}}_{\mu\nu} = 2 e^\mu \kappa^\nu \sigma_{\mu\nu}$ in (4). In the FLRW limit, the only nonzero coefficient is the Ricci focusing term, and the integrand (4) reduces to $\Pi \overset{\text{FLRW}}{\to} -\frac{1}{3} u^\mu u^\nu R_{\mu\nu}$.

III. MODEL SETUP AND LIGHT PROPAGATION

In this section we describe the details of our numerical analysis. In Sec. III A we specify the LTB model that we investigate. In Sec. III B we detail the geodesic equations for light propagation and discuss the initial conditions used for specifying the light beams.

A. Parametrization of the Lemaître-Tolman-Bondi structure

The solution of the LTB metric specified in Sec. II B is determined by two independent components of the Einstein field equation which can be integrated to yield

$$(\partial_t A(t,r))^2 = \frac{2M(r)}{A(t,r)} - k(r) \quad (8)$$

and

$$\frac{\partial_r M(r)}{4\pi G A^2(t,r)\partial_r A(t,r)} = \rho, \quad (9)$$

where the integration constant $M(r)$ is the active gravitational mass inside a shell of radius r of the LTB structure. Equation (8) can be solved for $A(t,r)$ for valid specifications of the functions $M(r)$ and $k(r)$, specifications of the functions $M(r)$, $k(r)$ and initial conditions for $A(t,r)$. We impose that the big bang happens synchronously in the model by requiring that the big bang function

$$t_B(r) = t - \int_0^{A(t,r)} \mathrm{d}\tilde{A} \frac{1}{\sqrt{\frac{2M(r)}{\tilde{A}} - k(r)}} \quad (10)$$

is zero for all r.[2] We furthermore choose the spatial curvature profile such that

$$k(r) = \begin{cases} -1.3\times 10^{-7} r^2 \left(\left(\frac{r}{r_b}\right)^m - 1\right)^6 & \text{if } r < r_b \\ 0 & \text{otherwise,} \end{cases} \quad (11)$$

where r_b is the radius of the LTB structure, outside of which the curvature is that of an Einstein de Sitter (EdS), which we shall refer to as the background metric. The condition $t_B(r) = 0$ and the profile (11) yield a closed-form solution to (8) in terms of t, r and $M(r)$; see [31] or Appendix A in [32]. The function $M(r)$ can be specified through a suitable choice of initial conditions for $A(t,r)$ [31], which in turn specifies $A(t,r)$ throughout. Here we choose the EdS-adapted initial conditions with $A(t_i, r) = a_{\mathrm{EdS}}(t_i) r$, where $a_{\mathrm{EdS}}(t_i) = (t_i/t_0)^{2/3}$ and $t_0 = 2/3/H_0$, with the initial scale

[2]Note that this integral can be solved explicitly. Solutions are given in, e.g., [28], but for our work we found it convenient to solve the ODE (8).

factor $a_{\mathrm{EdS}}(t_i) = 1/1100$ and with the initial time t_i fixed by $H_0 = 70$ km/s/Mpc.

The curvature model (11) represents a central void surrounded by a steep overdensity. We used $r_b = 40$ Mpc for all numerical computations. The choice $m = 6$ was used during the main part of our study, but to test the significance of the exact density profile on our results, we have also studied a single light ray passing through a structure with $m = 2$. In addition, we have made minor tests using different void depths and sizes of the surrounding overdensity by scaling the function $k(r)$. We find that the results do not qualitatively depend on the exact choice of density profile, but note that for a more significant change in density profile, the results should be expected to differ even qualitatively. For instance, this is seen by the comparisons in the Appendix of [16], which reveal that a prominent deviation from the FLRW result can be expected if the LTB inhomogeneity does not reduce *exactly* to an FLRW background at a reasonably small value of r. We also note that the strongest signs of inhomogeneity appear at the edges of the LTB structure, where the density contrast is at its steepest.

B. Light propagation and initial conditions

We choose a comoving observer located in the EdS region of the spacetime with a worldline passing through the point $\mathcal{O}$ given by the time coordinate $t_{\mathcal{O}} = 2/3/H_0$ with $H_0 = 70$ km/s/Mpc, corresponding to the present time in our model. The radial coordinate is chosen such that the observer is located 10 Mpc outside of the structure: $r_{\mathcal{O}} = r_b + 10$ Mpc, and the angular coordinates $\theta_{\mathcal{O}}$, $\phi_{\mathcal{O}}$ are fixed arbitrarily.

For each central null ray,[3] we choose a random line of sight with equal probability for all directions on the observer's sky. Upon transformation to spherical coordinates, this determines initial values of k^r, k^θ, and k^ϕ (and we always require $k^r > 0$). With this procedure, some light rays will miss the LTB structure and only propagate through EdS spacetime. We remove these rays from the analysis so that they do not, e.g., contribute to computations of mean quantities. The spatial direction vector is normalized in accordance with the initial condition of k^t which can be chosen arbitrarily without loss of generality. To compute the components of $\boldsymbol{\kappa}$ along the central null ray, we need the partial derivatives of the tangent vector along the ray. We use the procedure detailed in [15]; i.e., we solve

$$\frac{dk^\mu_{,\nu}}{d\lambda} = \frac{\partial}{\partial x^\nu}\frac{dk^\mu}{d\lambda} - k^\beta_{,\nu}k^\mu_{,\beta} \tag{12}$$

simultaneously with the geodesic equation

$$\frac{d}{d\lambda}(g_{\alpha\beta}k^\beta) = -\frac{1}{2}g_{\mu\nu,\alpha}k^\mu k^\nu. \tag{13}$$

The solution to the system of Eqs. (12) and (13) is specified by the initial conditions for k^μ described above, along with initial conditions for $k^\mu_{,\nu}$. These initial conditions uniquely define a 4-dimensional congruence of null geodesic rays around the central null ray.

We are interested in computing the redshift drift corresponding to comoving emitters, but we do not know *a priori* the initial conditions for $k^\mu_{,\nu}$ that correspond to a comoving emitter passing through a given event of emission $\mathcal{E}$ along the central null ray.[4] We thus follow an empirical approach, where we first define a bundle of null rays and then assess whether emitters of the incoming light rays on the observer worldline (almost) correspond to comoving emitters. For this purpose, we choose initial conditions for the null bundle such that $\boldsymbol{\kappa}_{\mathcal{O}} = \mathbf{0}$; i.e., the emitting sources are constrained to remain at a fixed direction on the observer's sky. This choice of initial condition is compatible with setting $k^\mu_{,t}|_{\mathcal{O}} = \frac{1}{k^t}\frac{dk^\mu}{d\lambda}|_{\mathcal{O}}$ in the LTB adapted coordinate system. The remaining initial conditions $k^\mu_{,i}|_{\mathcal{O}}$ must be compatible with this choice and the geodesic requirement (13), but are otherwise gauge choices of the signal arriving at the observer worldline.[5] Following [15], we set $k^\mu_{,i}|_{\mathcal{O}} = 0$ in Cartesian coordinates before making a coordinate transformation to spherical coordinates. We summarize our choice of initial conditions as follows:

$$k^\mu_{,t}|_{\mathcal{O}} = \frac{1}{k^t}\left.\frac{dk^\mu}{d\lambda}\right|_{\mathcal{O}}, \qquad k^\mu_{,i}|_{\mathcal{O}} = 0, \qquad i = x, y, z. \tag{14}$$

When the light rays travel exclusively in the FLRW region, the initial conditions (14) are compatible with comoving sources as emitters of the signal. However, once light enters the LTB structure, these initial conditions will generally not be compatible with comoving emitters since only radial light rays are repeatable in LTB models (see, e.g., [33]). However, emitters of the light contained in the bundle might nevertheless be *close* to being comoving.

As discussed in detail in Appendix B, we can determine the family of 4-velocity fields of sources which are candidates for having emitted the light with incoming conditions (14) at the observer. The 4-velocity of the source can be chosen uniquely from specifying α in (B2). Here we make the following choice of 4-velocity:

[3]We use the term "central null ray" to describe the light ray which passes between the primary points of emission $\mathcal{E}$ and observation $\mathcal{O}$, and around which we consider the extension into a congruence of null rays (see below).

[4]In principle, we could solve for the appropriate photon congruence description connecting a given emitter worldline with the observer worldline, by solving the geodesic deviation equation with Dirichlet boundary conditions as specified in Sec. 3.1 of [19]. However, in practice, it is computationally heavy to solve this boundary value problem for each point along the central null ray.

[5]See Appendix B for further discussions on the gauge choices involved with the initialization of the geodesic null bundle.

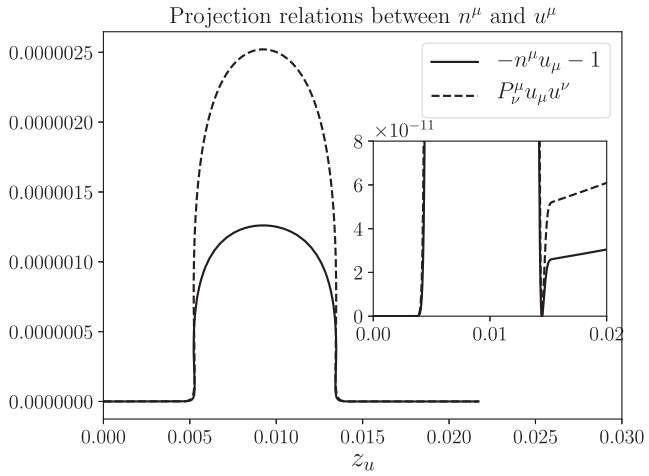

FIG. 1. Projection of u^μ orthogonal to n^μ and k^μ using the projection tensor, together with projection of u^μ along n^μ along a single light ray.

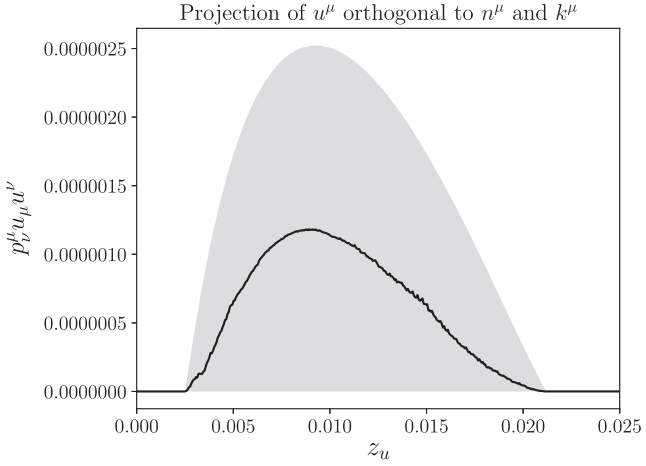

FIG. 2. Projection of u^μ orthogonal to n^μ and k^μ using the projection tensor. The black line indicates the mean over 1400 light rays while the grey-shaded area indicates the spread. The result is plotted against the redshift of comoving emitters.

$$n^\mu \equiv \frac{X^\mu_{\rm scr}}{\sqrt{-g_{\nu\rho}X^\nu_{\rm scr}X^\rho_{\rm scr}}}, \qquad X^\mu_{\rm scr} = \tilde{X}^\mu + \alpha_{\rm scr}k^\mu, \tag{15}$$

where $\tilde{\boldsymbol{X}}$ is determined by (B3) and where $\alpha_{\rm scr} \equiv \tilde{X}^\mu e_\mu / E_u$. We label the photon energy $E_u \equiv -k^\mu u_\mu$ with a subscript from now on to distinguish the energy measured in the LTB comoving frame from the energy as measured in other frames. This choice of sources ensures that the spatial direction of propagation of the photon $\boldsymbol{e}$ as seen in the comoving LTB frame is indeed also spatial in the frame of the source, i.e., $n^\mu e_\mu = 0$. Thus, any difference between $\boldsymbol{u}$ and $\boldsymbol{n}$ is due to the components of $\boldsymbol{u}$ in the screen space orthogonal to the 2-dimensional congruence of light spanned by $\boldsymbol{k}$ and $\tilde{\boldsymbol{X}}$, hence the use of the subscript scr which is short for "screen space".

The emitter 4-velocity field n^ν turns out to be very close to the comoving 4-velocity field u^μ at every point along the central null ray. This can be seen by computing the norm of $\boldsymbol{u}$ in the screen space orthogonal to $\boldsymbol{n}$ and $\boldsymbol{k}$: $P^{\mu\nu}u_\mu u_\nu$, with $P^\mu_\nu \equiv \frac{-k^\mu k_\nu}{E_n^2} + \frac{k^\mu n_\nu}{E_n} + \frac{n^\mu k_\nu}{E_n} + g^\mu_\nu$. Alternatively, we could compute the relative tilt $-n^\mu u_\mu$. We show both closeness measures in Fig. 1 for a fiducial light ray. As seen, the two measures are very similar and indeed, in general, differ by a factor of 2 at lowest order[6] in $\boldsymbol{v}$; therefore, we analyze the former measure only for the full set of null rays. The projection $P^{\mu\nu}u_\mu u_\nu$ is shown for 1400 light rays in Fig. 2. As seen, the projection is small—at most of order 10^{-6}, and of order 10^{-10} for emitters in the FLRW region (on the opposite side of the structure as compared to the observer)—which means that the relative velocity between $\boldsymbol{n}$ and $\boldsymbol{u}$ is at most of order 10^{-3} and reaches levels of order 10^{-5} once the structure has been traversed. Thus, comoving emitters are *close to* being emitters of the light signal received at the observer worldline, even when being situated within the structure. We thus expect the redshift drift signal in the comoving frame to be close to that in the frame of $\boldsymbol{n}$.

In the following we analyze the redshift drift signal in the frame of the almost-comoving geodesic observers generated by the 4-velocity $\boldsymbol{n}$. Similarly to the expression for the redshift drift used in [15], we can compute the redshift drift corresponding to the geodesic emitter with 4-velocity n^μ as (see Appendix B for details)

$$\delta z_n \equiv -\delta t_{\mathcal{O}} \cdot \left(\frac{E_n}{E^2_{\mathcal{O}}} k^t_{,t}|_{\mathcal{O}} + \frac{1}{E_n} n^\mu n^\mu \nabla_\mu k_\nu \right), \tag{16}$$

where $E_n \equiv -k^\mu n_\mu$, and where evaluation is at any point along the central null ray.

In addition, we make use of the following convenient approximation of δz_n:

$$\begin{aligned}\delta z_u &\equiv -\delta t_{\mathcal{O}} \cdot \left(\frac{E_u}{E^2_{\mathcal{O}}} k^t_{,t}|_{\mathcal{O}} + \frac{1}{E_u} u^\mu u^\mu \nabla_\mu k_\nu \right) \\ &= \frac{\delta t_{\mathcal{O}}}{k^t_{\mathcal{O}}} \left(-(1+z_u) k^t_{,t|\mathcal{O}} + \frac{k^t_{,t|\mathcal{E}}}{1+z_u} \right),\end{aligned} \tag{17}$$

which, in the following section, we verify remains close to δz_n. The approximation (17) can conveniently be written as the integral representation (3) with integrand (4) and coefficients (7).

[6]It can be verified that $P^{\mu\nu}u_\mu u_\nu = v^\mu v_\mu + \mathcal{O}(v^3)$, where v^μ is the relative velocity defined through $u^\mu = (n^\mu + v^\mu)/\sqrt{1 - v^\nu v_\nu}$. Thus, we have the following relation: $P^{\mu\nu}u_\mu u_\nu = 2(-n^\mu u_\mu - 1) + \mathcal{O}(v^3)$.

IV. RESULTS

In this section we present the results obtained by propagating light rays through a single LTB structure, as described in Sec. III. In Sec. IV A we present results obtained by considering a single random light ray. Afterwards we move on to present results obtained from 1400 light rays in Sec. IV B.

A. Single light ray

In this section we show results from propagating a single light ray with a random impact parameter through the LTB structure. We set $\delta t_{\mathcal{O}} = 30$ years, where $\delta t_{\mathcal{O}}$ is the observer's proper time elapsed between two measurements of the redshift and δz is the drift (change) in the redshift of a source during that interval. We show results using the density profile defined by $m = 6$, but we have verified that the results are similar for the profile corresponding to $m = 2$ as well as for models with different scalings of $k(r)$ to enhance or suppress the structure.

We compute the redshift drift signal in the frame of the geodesic and almost-comoving emitters with 4-velocity field $\boldsymbol{n}$, as detailed in Sec. III B and compare the exact redshift drift signal of these emitters (16) to the approximation (17). This comparison is shown in Fig. 3 where it is seen that the deviation between δz_u and δz_n is maximally of order 10^{-3}, as is also expected based on Fig. 2. We thus find that δz_u is a good approximation of δz_n along the entire null ray—a result which we verify holds for the full sample of null rays considered in our analysis—and we use δz_u as a convenient approximation of the redshift drift signal in the following.

Figure 4 shows the contributions of the multipole components in the representation (4) together with the total redshift drift signal approximation (17), with initial conditions for the light bundle as specified in Sec. III B. We

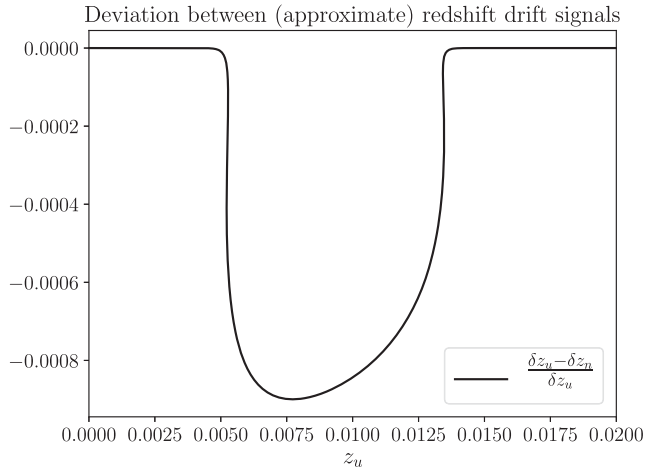

FIG. 3. Deviation between two redshift drifts along a fiducial light ray.

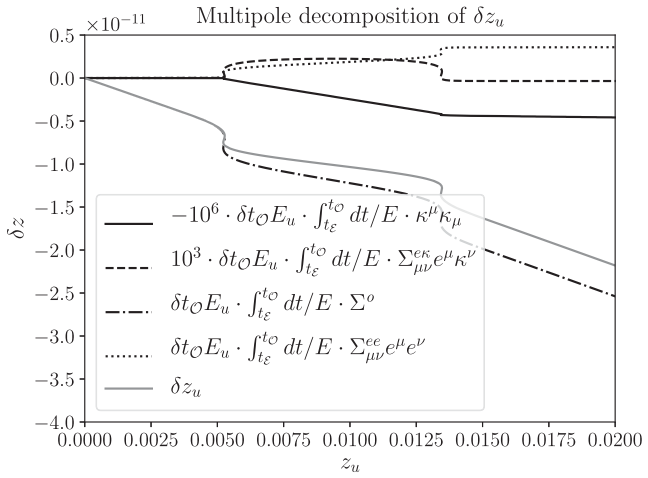

FIG. 4. Individual components of the redshift drift signal along a light ray. The two subdominant components are scaled to ease assessment of their qualities.

immediately see that the two main contributions are those corresponding to the Ricci and Weyl tensors. This is encouraging since these two terms do not depend on the extension of the congruence k^μ_ν away from the central null ray, and are thus much more easily computed than the (integral of the) two terms $-\kappa^\mu \kappa_\mu$ and $e^\mu \kappa^\nu \Sigma^{e\kappa}_{\mu\nu} = 2 e^\mu \kappa^\nu \sigma_{\mu\nu}$ in (4).

The contribution from the drift κ is actually so small that it is nearly swamped by the numerical errors of the computations which make our redshift drift determinations reliable only at the level of 4 significant digits. With this precision, we are just barely able to see the contribution from the next-smallest term, the shear term. This is illustrated in Fig. 5 where we show the relative difference between δz_u and the approximate redshift drift computed using only the two or three dominant multipole contributions, respectively. We see that the approximation $\delta z_{\text{Weyl+Ricci+shear}} \equiv E \int_{t_\mathcal{E}}^{t_\mathcal{O}} dt/E \Sigma^o + \Sigma^{ee}_{\mu\nu} e^\mu e^\nu + \Sigma^{e\kappa}_{\mu\nu} = 2\sigma_{\mu\nu} e^\mu \kappa^\nu$, using the three dominant multipole contributions, gives an accurate determination of δz_u within the numerical errors, a rough estimate of which is shown as a shaded area. The integral term involving $-\kappa^\mu \kappa_\mu$ is roughly 2 orders of magnitude smaller than what can be resolved within the numerical errors of this analysis, and might thus be neglected for all practical purposes.

We note that the Weyl contribution to the redshift drift signal is significant—also for emitters placed outside of the LTB structure (on the opposite side of the observer). However, the Weyl contribution can be both positive and negative, so the mean Weyl contribution may be modest when averaging over many individual light rays with different impact parameters. Figure 6 shows the Weyl contribution along two arbitrarily chosen fiducial rays with positive and negative Weyl contributions, respectively. The contributions are shown together with the

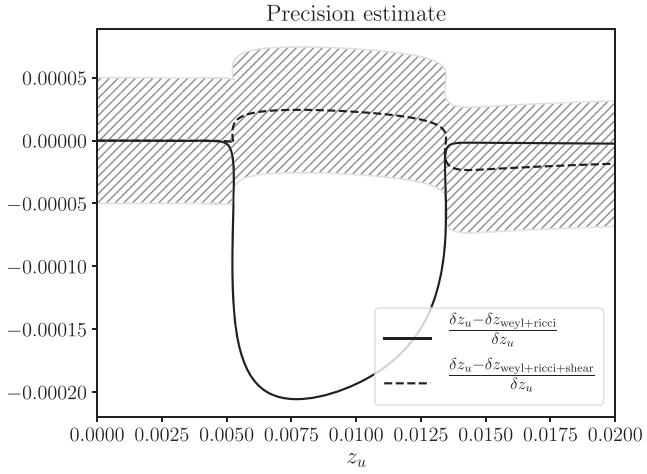

FIG. 5. Deviations between δz_u and two approximations computed by including the two and three most dominant multipole contributions—either Weyl + Ricci or Weyl + Ricci + shear components, corresponding to $\delta z_{\text{Weyl+Ricci}} \equiv E\int_{t_\mathcal{E}}^{t_\mathcal{O}} dt/E\Sigma^o + \Sigma^{ee}_{\mu\nu}e^\mu e^\nu$ and $\delta z_{\text{Weyl+Ricci+shear}} \equiv E\int_{t_\mathcal{E}}^{t_\mathcal{O}} dt/E\Sigma^o + \Sigma^{ee}_{\mu\nu}e^\mu e^\nu + \Sigma^{e\kappa}_{\mu\nu} = 2\sigma_{\mu\nu}e^\mu\kappa^\nu$, respectively. The shaded area indicates a rough estimate of the numerical precision of the computations, corresponding to 4 significant digits.

density profile along the individual rays to illustrate that the negative Weyl contribution appears to occur when light rays move further into the underdense region of the structure. Although it is not clearly visible in the figure, we note that the redshift is nonmonotonous along both rays.

Before moving on to discuss the results obtained when averaging over several light rays, we note that a simple relation between the redshift drift and the local expansion rate along light rays is *not* apparent. Indeed, in the absence of certain systematic impacts of anisotropies along the central null ray, the redshift drift signal is expected to simplify to an expression similar to the FLRW relation [8]

$$\delta z_{\text{simple}} \equiv \delta t_\mathcal{O}((1+z)\mathfrak{H}_\mathcal{O} - \mathfrak{H}), \tag{18}$$

with the generalized "Hubble parameter" $\mathfrak{H} \equiv \frac{1}{3}\theta + e^\mu e^\nu \sigma_{\mu\nu}$ describing the rate of expansion of length scales along the direction of the photon 4-momentum. However, Fig. 7 shows that (18) is not a good approximation for emitters located within the LTB structure. The approximation δz_{simple} departs from δz_u by orders of magnitude for most emitters located within the LTB structure, which might be assigned to both the large departures of θ from the EdS background expansion rate for most points within the LTB structure and to the projected shear contribution within the structure. This is illustrated in Fig. 4 along a fiducial light ray. For emitters located in the FLRW region (on the opposite side of the structure from the observer), Eq. (18) provides an extremely good approximation as it is simply the background EdS redshift drift which δz_u reduces to outside of the structure, to the precision of our computations (around 5 significant digits).

B. Multiple light rays

In this section, we redo the analysis for 1400 light rays and compute the mean value and spread of the results. The observer is always the same (placed at $t = t_\mathcal{O}$ and $r = r_b + 10$ Mpc). Each light ray is propagated until it reaches $z = 0.025$, which is enough to traverse the entire LTB structure.

Figure 8 shows the integrated multipole components of the redshift drift. It is visible from the figure that the two components which depend on the drift of the viewing angle, $\boldsymbol{\kappa}$, are subdominant and can, to a high precision, be neglected, as we also found for the single light ray above. This means that we can, to a good precision, approximate the redshift drift signal from the Ricci and electric Weyl curvature components along the individual null rays. The figure also shows that the Weyl contribution does not

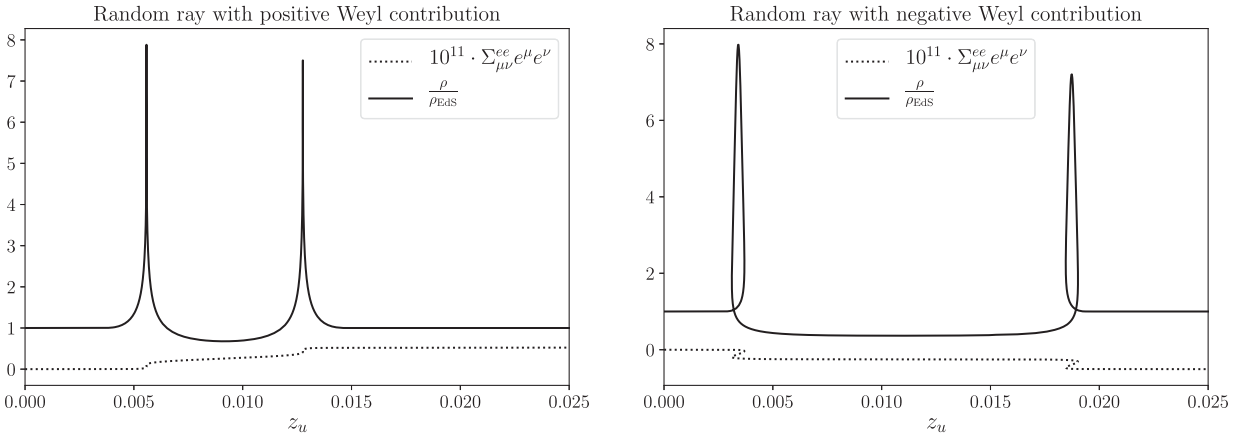

FIG. 6. Weyl contributions to the redshift drift along fiducial light rays with opposite sign of the Weyl contribution. The contributions are shown together with the density profiles along the light rays.

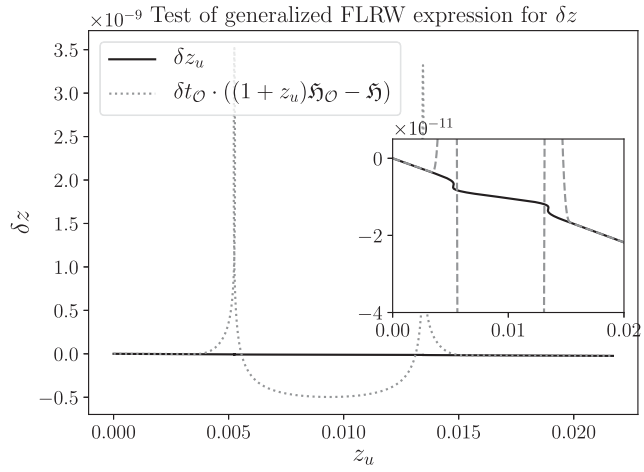

FIG. 7. Actual redshift drift compared with simple expectation based on generalized FLRW relation along a single light ray. A close-up is included since the simple approximation is several orders of magnitude larger than the actual redshift drift several places along the light rays.

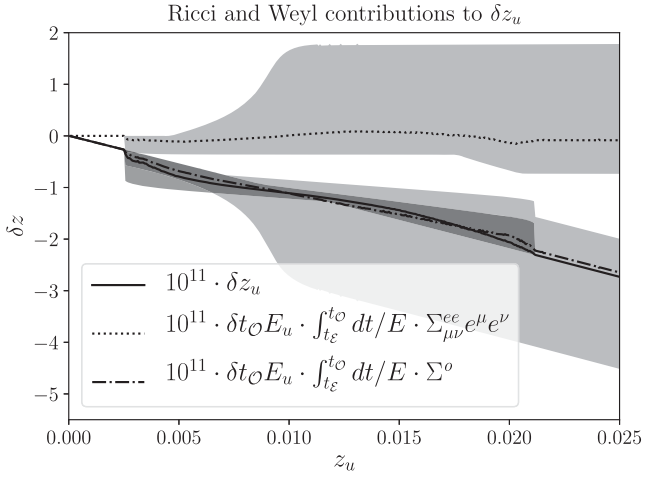

FIG. 9. Ricci and Weyl contributions to the redshift drift along 1400 light rays. The black lines indicate mean values while the shaded areas indicate the spread.

vanish on average after traversal of the light ray through the structure, but the remaining mean effect is much smaller than the contribution from the average Ricci term, with the mean of the former making up approximately 5% of the signal after traversal of the entire structure. This is also seen in Fig. 9, which shows the mean and spread of the Ricci and Weyl contributions together with the total redshift drift signal.

In Fig. 10, we show the deviations between δz_u and the signal corresponding to the redshift drift without the $\boldsymbol{\kappa}$-contributions, as well as the difference between δz_u and δz_n. Both of the differences are subpercentage, again indicating that we can, to a good approximation, treat the sum of the Ricci and Weyl contributions to the redshift drift as *the* redshift drift signal measured by a comoving observer in the FLRW region and emitted by comoving sources along the light paths.

Lastly, Fig. 11 shows the difference between the mean redshift drift and the EdS (background) redshift drift. The difference becomes quite large for typical emitters of light, emphasizing the potential importance of taking effects of structures into account when interpreting real upcoming redshift drift data. However, we note that the relative departures from the EdS signal are expected to decrease for longer distances of light propagation than a single LTB structure.

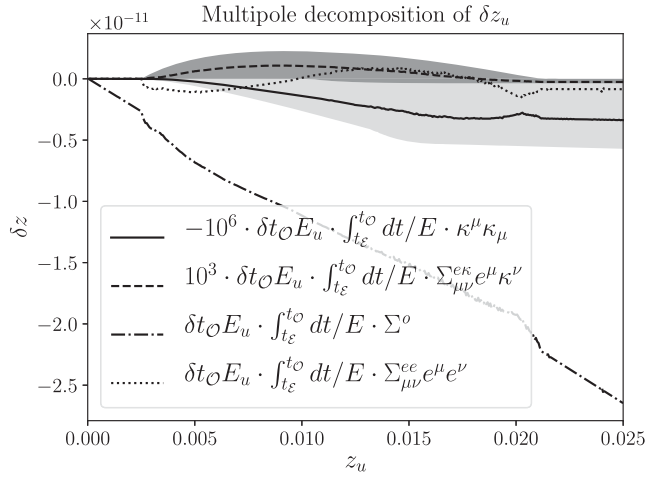

FIG. 8. Mean of individual components of the redshift drift signal along 1400 light rays. The two subdominant components are scaled to ease assessment of their qualities and are shown together with their spreads (shaded areas).

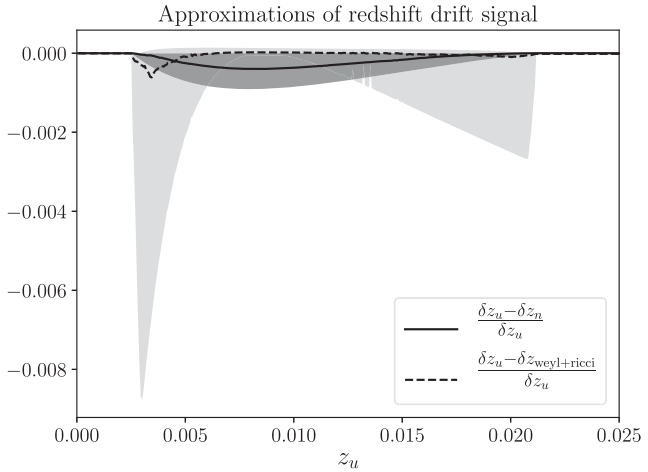

FIG. 10. Deviation between redshift drifts δz_u and δz_n as well as between δz_u and the redshift drift computed without the $\boldsymbol{\kappa}$-contributions, i.e., $\delta z_{\mathrm{Weyl+Ricci}} \equiv E\int_{t_\mathcal{E}}^{t_\mathcal{O}} dt/E\Sigma^o + \Sigma^{ee}_{\mu\nu}e^\mu e^\nu$. The black lines indicate mean values while the spreads are indicated by shaded areas.

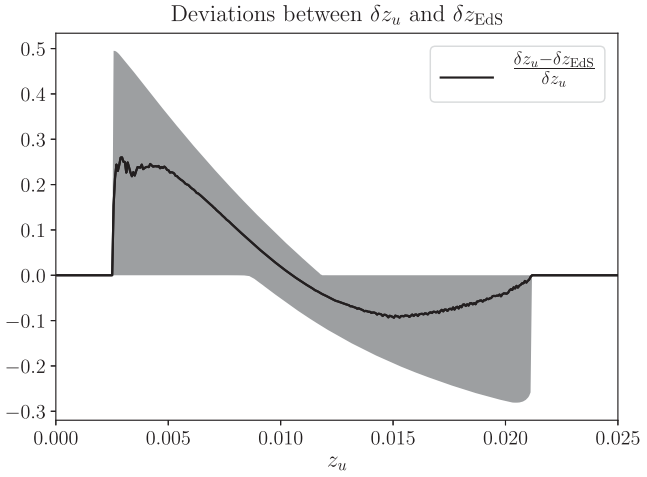

FIG. 11. Deviation between δz_u and the background (EdS) redshift drift. The line indicates the difference between the EdS redshift drift and the mean redshift drift while the shaded area indicates the spread.

For the comparison in Fig. 11, we compute the EdS redshift drift as

$$\delta z_{\mathrm{EdS}} = (1 + z_u(\lambda_{\mathcal{E}}))H_0 - H(z_u(\lambda_{\mathcal{E}})), \tag{19}$$

where $H(z_u)$ is the background EdS Hubble parameter function as parametrized in terms of EdS redshift z_{EdS} and evaluated at the value $z_{\mathrm{EdS}} = z_u$. We note that, since the local difference between $z_{\mathrm{EdS}}(t(\lambda))$ and $z_u(\lambda)$ is subpercentage along the null rays, the result does not change significantly if we instead use an EdS parametrization in terms of the time parameter of emission:

$$\delta z_{\mathrm{EdS}}^{\mathrm{alternative}} = (1 + z_{\mathrm{EdS}}(t_{\mathcal{E}}))H_0 - H(z_{\mathrm{EdS}}(t_{\mathcal{E}})), \tag{20}$$

and compute the difference between δz_u and $z_{\mathrm{EdS}}^{\mathrm{alternative}}$ at equal values of $\lambda_{\mathcal{E}}$ (or $t_{\mathcal{E}}$) instead of equal values of redshift.

Note also that the steep edges of the shaded area in this as well as other figures are not actually vertical but merely very steep, corresponding to the steep density profile of the studied model.

V. CONCLUSION

We considered a formalism for computing the redshift drift in a general spacetime with an arbitrary observer and arbitrary emitting sources, and we investigated the special case of an LTB model. We pointed out the importance of the position drift of the photons arriving at the observer and that different values of position drift correspond to different potential emitters of the signal. For the LTB model we find that the contributions to the redshift drift from terms involving the drift of the viewing angle of light are several orders of magnitude smaller than the dominant Ricci and Weyl contributions. We can therefore, to a good approximation, neglect these complicating factors. Since we find that the drift of the viewing angle almost vanishes once the ray has traversed the LTB structure, cumulative effects must be small. Hence, we expect the redshift drift signal to be dominated by its Ricci and Weyl contributions, also in Swiss-cheese models based on LTB structures, but defer a detailed study of this point to upcoming work. Based on the similarities regarding the redshift behaviors in LTB and Szekeres models as studied in, e.g., Sec. IV A in [34], we also expect the result to hold for quasispherical Szekeres models and the corresponding Swiss-cheese models.

We considered the mean redshift drift signal for 1400 light rays with random impact parameters relative to the LTB structure. The mean redshift drift is dominated by the Ricci contribution, but we note that the mean Weyl contribution has an importance of around 5%, even in the FLRW region after the light rays have traversed the structure. We also note that inside the inhomogeneous region, the redshift drift associated with typical emitters deviates by several tens of percent from the "background" FLRW value. Although we expect such deviations to become less pronounced when light travels over greater distances, this indicates that the local effect of structures on the redshift drift signal may need attention when dealing with upcoming real data.

ACKNOWLEDGMENTS

We wish to thank Mikołaj Korzyński for valuable comments. A. H. acknowledges funding from the European Research Council (ERC) under the European Union's Horizon 2020 research and innovation programme (Grant Agreement ERC Advanced Grant No. 740021–ARTHUS, PI: Thomas Buchert). S. M. K. is funded by the Carlsberg Foundation. The open source computer algebra system Maxima was used to verify computations of Christoffel symbols and Riemann tensors for the LTB metric. Some of the computations done for this project were performed on the UCloud interactive HPC system, which is managed by the eScience Center at the University of Southern Denmark.

APPENDIX A: MULTIPOLE COMPONENTS FOR THE LTB MODEL

In this appendix, we provide a list with the explicit multipole components of Eq. (7) for the LTB model together with the explicit components of the drift of the viewing angle, $\boldsymbol{\kappa}$.

For a random light ray, the components of $\boldsymbol{\kappa}$ are, for the LTB metric, given by

$$
\begin{aligned}
\kappa^t &= 0 \\
\kappa^r &= -\frac{1}{k^t}\left[\left(1-R\frac{(k^r)^2}{(k^t)^2}\right)\left(k^r_{,t}+\frac{R_{,t}}{2R}k^r\right)-\frac{k^r k^\theta}{(k^t)^2}A^2\left(k^\theta_{,t}+\frac{A_{,t}}{A}k^\theta\right)-\frac{k^r k^\phi}{(k^t)^2}A^2\sin^2(\theta)\left(k^\phi_{,t}+\frac{A_{,t}}{A}k^\phi\right)\right] \\
\kappa^\theta &= -\frac{1}{k^t}\left[-\frac{k^\theta k^r}{(k^t)^2}R\left(k^r_{,t}+\frac{R_{,t}}{2R}k^r\right)+\left(1-\frac{(k^\theta)^2}{(k^t)^2}A^2\right)\left(k^\theta_{,t}+\frac{A_{,t}}{A}k^\theta\right)-\frac{k^\theta k^\phi}{(k^t)^2}A^2\sin^2(\theta)\left(k^\phi_{,t}+\frac{A_{,t}}{A}k^\phi\right)\right] \\
\kappa^\phi &= -\frac{1}{k^t}\left[-\frac{k^\phi k^r}{(k^t)^2}R\left(k^r_{,t}+\frac{R_{,t}}{2R}\right)-\frac{k^\phi k^\theta}{(k^t)^2}A^2\left(k^\theta_{,t}+\frac{A_{,t}}{A}k^\theta\right)+\left(1-\frac{(k^\phi)^2}{(k^t)^2}A^2\sin^2(\theta)\right)\left(k^\phi_{,t}+\frac{A_{,t}}{A}k^\phi\right)\right],
\end{aligned}
\tag{A1}
$$

from which the multipole term $-\kappa^\mu\kappa_\mu$ follows trivially. Using the Einstein equation, the monopole term of the redshift drift can simply be written as

$$
\Sigma^o = -\frac{1}{3}u^\mu u^\nu \mathcal{R}_{\mu\nu} = -\frac{4\pi G}{3}\rho. \tag{A2}
$$

This is the dominant redshift contribution for the considered setup. The other significant term is given by

$$
\begin{aligned}
\Sigma^{ee}_{\mu\nu}e^\mu e^\nu &= -u^\rho u^\sigma C_{\rho\mu\sigma\nu}e^\mu e^\nu \\
&= -(C_{trtr}e^r e^r + C_{t\theta t\theta}e^\theta e^\theta + C_{t\phi t\phi}e^\phi e^\phi),
\end{aligned}
\tag{A3}
$$

with

$$
C_{trtr} = -\frac{1}{2}R_{,tt}+\frac{1}{4}\frac{R^2_{,t}}{R}-\frac{4}{3}\pi G\rho R, \tag{A4}
$$

$$
C_{t\theta t\theta} = -AA_{,tt}-\frac{4}{3}\pi G\rho A^2, \tag{A5}
$$

$$
C_{t\phi t\phi} = -AA_{,tt}\sin^2(\theta)-\frac{4}{3}\pi G\rho A^2\sin^2(\theta). \tag{A6}
$$

Finally, the shear term, which turns out to be negligible in the considered setup, is given by

$$
\begin{aligned}
\Sigma^{e\kappa}_{\mu\nu}e^\mu\kappa^\nu &= 2\sigma_{\mu\nu}e^\mu\kappa^\nu \\
&= \frac{2}{3}\Sigma(-2Re^r\kappa^r + A^2e^\theta\kappa^\theta + \sin^2(\theta)A^2e^\phi\kappa^\phi),
\end{aligned}
\tag{A7}
$$

where $\Sigma \equiv \frac{A_{,t}}{A}-\frac{A_{,tr}}{A_{,r}}$.

APPENDIX B: GEODESIC DEVIATION AND DRIFT EFFECTS

In the study of drift effects, we are interested in following the same emitter over time and considering the temporal change in various observable signals associated with that emitter. In order to describe drift signals in mathematical detail, we thus need to define a connecting congruence of photons between the observer worldline and the emitters under consideration. There are two ways that we might approach the selection of an emitter as viewed from a given observer worldline: (i) we might simply consider *a priori* fixing the emitter worldline. This uniquely determines a connecting congruence of null rays in the absence of caustics; or (ii) we can consider a fixed congruence of photons intersecting the observer worldline and deduce the class of potential emitters that intersect this congruence with their worldlines. From this class we might further identify a unique emitter from an appropriate criterion.

There can be advantages of both approaches. For the purpose of explicit calculation, it can, in practice, be computationally difficult to construct the connecting null congruence between the observer and the fixed emitter as in the first approach. Thus, it is sometimes more convenient to take the second approach and simply consider the emitters that happen to intersect a given null congruence as initialized at the observer. We describe the latter approach here. See [19] for details on the first approach.

Let the observer of interest be represented by its worldline γ_o as generated by the 4-velocity $\boldsymbol{u}_o$. We consider a central null geodesic as received at the point of observation $\mathcal{O}$ on γ_o, and we further consider a bundle of null geodesics around this central null ray that form a nonintersecting congruence. We might consider an appropriate extension of the congruence along the observer worldline to form a two-dimensional congruence. We might also consider a small extension of the congruence in the space orthogonal to $\boldsymbol{u}_\mathcal{O}$ and the central incoming null ray in order to form a four-dimensional congruence of null rays. In any of the cases, there will be a 1-parameter family of null geodesics Γ_o with 4-momentum field $\boldsymbol{k}$ intersecting the observer's worldline γ_o. We might ask which emitters could have sent this family of photons that were later received by the observer. For a source to have emitted the null geodesics in Γ_o, its worldline must intersect the family of null lines of Γ_o. Formally, this is equivalent to demanding that the emitter 4-velocity is a deviation vector of Γ_o. Thus, we assume that a source worldline γ_e intersects the central null ray at a point $\mathcal{E}$; for this source to be an emitter of Γ_o, we require that its 4-velocity satisfies $u^\mu_\mathcal{E} = (E_\mathcal{E}/E_\mathcal{O})X^\mu_\mathcal{E}$, with $E = -k^\mu u_\mu$, and where X^μ is given by the propagation law

$$
k^\nu\nabla_\nu X^\mu - X^\nu\nabla_\nu k^\mu = \mu k^\mu, \qquad X^\mu_\mathcal{O} = u^\mu_\mathcal{O}, \tag{B1}
$$

where μ is an arbitrary function, only restricted by the requirement that X^μ remains timelike, representing the possible parametrizations of the rays (with affine parametrizations characterized by $k^\nu\nabla_\nu\mu = 0$). The choice of proportionality constant in $u^\mu_{\mathcal{E}} = (E_{\mathcal{E}}/E_{\mathcal{O}})X^\mu_{\mathcal{E}}$ is compatible with the conservation law $X^\mu k_\mu = (X^\mu k_\mu)_{\mathcal{O}} = -E_{\mathcal{O}}$ following from (B1). The solutions to (B1) can be reformulated as

$$X^\mu = \tilde{X}^\mu + \alpha k^\mu, \qquad k^\mu\nabla_\mu\alpha = \mu, \qquad \alpha_{\mathcal{O}} = 0, \tag{B2}$$

with $\tilde{X}^\mu$ given by the solution to the propagation law without a source term,

$$k^\nu\nabla_\nu\tilde{X}^\mu - \tilde{X}^\nu\nabla_\nu k^\mu = 0, \qquad \tilde{X}^\mu_{\mathcal{O}} = u^\mu_{\mathcal{O}}, \tag{B3}$$

such that $\tilde{X}^\mu$ obeys the usual geodesic deviation equation

$$k^\alpha\nabla_\alpha(k^\beta\nabla_\beta\tilde{X}^\mu) = R^\mu{}_{\alpha\beta\nu}k^\alpha k^\beta\tilde{X}^\nu, \tag{B4}$$

with a unique solution from the initial conditions $\tilde{X}^\mu_{\mathcal{O}} = u^\mu_{\mathcal{O}}$ and $\tilde{X}^\beta\nabla_\beta k^\mu|_{\mathcal{O}}$. The condition $\alpha > \tilde{X}^\mu\tilde{X}_\mu/E_{\mathcal{O}}/2$ ensures that X^μ is timelike. The class of possible emitters of the null congruence Γ_o as received by the observer is described by the class of tangent vectors given by (B2) and satisfying the timelike condition. Conversely, emitters with 4-velocities that are not proportional to any of the tangent vectors in class (B2) could *not* have emitted the photons of Γ_o, and describing the drift effects of such emitters thus requires considering other appropriate photon congruences.

In practice, for a given photon congruence, we might solve for the possible emitters of the photons intersecting the observer worldline by first solving (B3) and then considering the allowed class of transformations of the emitter tangent vector (B2). At each point along the central null ray, α might be chosen to uniquely determine an emitter 4-velocity $n^\mu = X^\mu/(-X^\nu X_\nu)^{\frac{1}{2}}$. For instance, α might be chosen in a way that maximizes $n^\mu U_\mu$ for a given preferred 4-velocity $\boldsymbol{U}$, which might not itself be intersecting Γ_o.

We note that for a given emitter associated with a solution X^μ to (B1), the position drift of the emitter on the observer's sky is

$$\begin{aligned}\kappa^\mu_{\mathcal{O}} \equiv p^\mu_\nu u^\alpha\nabla_\alpha e^\nu|_{\mathcal{O}} &= -p^\mu_\nu\frac{1}{E}u^\alpha\nabla_\alpha k^\nu|_{\mathcal{O}} + p^\mu_\nu a^\nu|_{\mathcal{O}} \\ &= -p^\mu_\nu\frac{1}{E}k^\alpha\nabla_\alpha X^\nu|_{\mathcal{O}} + p^\mu_\nu a^\nu|_{\mathcal{O}} \\ &= -p^\mu_\nu\frac{1}{E}k^\alpha\nabla_\alpha\tilde{X}^\nu|_{\mathcal{O}} + p^\mu_\nu a^\nu|_{\mathcal{O}}.\end{aligned} \tag{B5}$$

The last equality shows that the position drift is invariant under transformations of the source's tangent vector of the type (B2), and follows from (B2) and the orthogonality between k^μ and the screen space projector $p^\mu_\nu \equiv -\frac{k^\mu}{E}\frac{k_\nu}{E} + \frac{k^\mu}{E}u_\nu + u^\mu\frac{k_\nu}{E} + g^\mu_\nu$ as defined on the observer worldline. It follows that the position drift is determined by the initial conditions $u^\mu_{\mathcal{O}}$, $a^\mu_{\mathcal{O}}$, $k^\mu_{\mathcal{O}}$ and $u^\alpha\nabla_\alpha k^\mu|_{\mathcal{O}} = k^\alpha\nabla_\alpha\tilde{X}^\mu|_{\mathcal{O}}$. Physically, the observed angular drift of the source is independent of the exact points of emission along Γ_o, and the position drift signal is given entirely from the initialization of the congruence of null rays at the observer position.

For a given emitter 4-velocity $n^\mu \equiv X^\mu/(-X^\nu X_\nu)^{\frac{1}{2}}$ and associated photon energy $E_n \equiv -n^\mu k_\mu$, the redshift drift signal is

$$\begin{aligned}\left.\frac{dz}{d\tau_o}\right|_{\mathcal{O}} &= -\left.\frac{E_n|_{\mathcal{E}}}{E_{\mathcal{O}}}\frac{u^\mu_o\nabla_\mu E}{E}\right|_{\mathcal{O}} + \left.\frac{n^\mu\nabla_\mu E_n}{E_n}\right|_{\mathcal{E}} \\ &= -\frac{n^\mu k_\mu|_{\mathcal{E}}}{E_{\mathcal{O}}}\frac{(a^\mu_o k_\mu + u^\mu_o u^\nu_o\nabla_\mu k_\nu)|_{\mathcal{O}}}{E_{\mathcal{O}}} \\ &\quad + \left.\frac{a^\mu k_\mu + n^\mu n^\nu\nabla_\mu k_\nu}{n^\mu k_\mu}\right|_{\mathcal{E}},\end{aligned} \tag{B6}$$

with emitter and observer 4-accelerations given by $a^\mu \equiv n^\nu\nabla_\nu n^\mu$ and $a^\mu_o \equiv u^\nu_o\nabla_\nu u^\mu_o$. The emitter 4-acceleration is not constrained by the above geodesic deviation analysis and must be chosen independently. We are usually interested in setting the 4-accelerations to zero, corresponding to the case of physical emitters and observers that are subject only to gravitational physics. We can exploit that

$$\left.\frac{n^\mu n^\nu\nabla_\mu k_\nu}{(n^\mu k_\mu)^2}\right|_{\mathcal{E}} = \frac{1}{E^2_{\mathcal{O}}}X^\mu X^\nu\nabla_\mu k_\nu = \frac{1}{E^2_{\mathcal{O}}}\tilde{X}^\mu\tilde{X}^\nu\nabla_\mu k_\nu \tag{B7}$$

to rewrite (B6) as

$$\begin{aligned}\left.\frac{dz}{d\tau_o}\right|_{\mathcal{O}} = -\frac{n^\mu k_\mu|_{\mathcal{E}}}{E_{\mathcal{O}}}\Bigg[&\frac{(a^\mu_o k_\mu + u^\mu_o u^\nu_o\nabla_\mu k_\nu)|_{\mathcal{O}}}{E_{\mathcal{O}}} \\ &- \frac{(E^2_{\mathcal{O}}a^\mu k_\mu/(n^\mu k_\mu)^2 + \tilde{X}^\mu\tilde{X}^\nu\nabla_\mu k_\nu)|_{\mathcal{E}}}{E_{\mathcal{O}}}\Bigg].\end{aligned} \tag{B8}$$

Thus, the final redshift drift signal depends only on the components of $\nabla_\mu k_\nu$ as projected onto the canonical deviation vector $\tilde{X}^\mu$. The evolution of the velocity vector $\tilde{X}^\mu\nabla_\mu k_\nu$ can in turn be calculated along the central null ray from the geodesic deviation equation (B4), where the right-hand side is known once $\tilde{X}^\mu$ is determined from the initial conditions $\tilde{X}^\mu_{\mathcal{O}} = u^\mu_{\mathcal{O}}$ and $u^\alpha\nabla_\alpha k^\mu|_{\mathcal{O}}$. Thus, the final expression for redshift drift depends only on the initial conditions for $u^\mu_{\mathcal{O}}$, $a^\mu_{\mathcal{O}}$, $k^\mu_{\mathcal{O}}$ and $u^\alpha\nabla_\alpha k^\mu|_{\mathcal{O}}$ together with $a^\mu_{\mathcal{E}}$ and the transforming parameter $\alpha_{\mathcal{E}}$. The latter parameter determines the photon energy as evaluated at the emitter $E_n|_{\mathcal{E}} = -n^\mu k_\mu|_{\mathcal{E}}$.

The expression (B8) makes it explicit that the redshift drift signal depends only on the extension of k^μ on the observer's worldline through $u^\alpha \nabla_\alpha k^\mu|_{\mathcal{O}}$ and does *not* depend on the initialization of any of the other independent components[7] of $\nabla_\mu k_\nu$. Any intermediate calculation making use of these should thus cancel for the final redshift drift signal.

[7]The components of $\nabla_\mu k_\nu|_{\mathcal{O}}$ are constrained by the null requirement $k^\nu \nabla_\mu k_\nu = 0$ and the geodesic requirement $k^\mu \nabla_\mu k^\nu = 0$.

[1] A. Sandage, The change of redshift and apparent luminosity of galaxies due to the deceleration of selected expanding universes, Astrophys. J. **136**, 319 (1962).

[2] G. C. McVittie, Appendix to the change of redshift and apparent luminosity of galaxies due to the deceleration of selected expanding universes, Astrophys. J. **136**, 334 (1962).

[3] J. Liske *et al.*, Cosmic dynamics in the era of extremely large telescopes, Mon. Not. R. Astron. Soc. **386**, 1192 (2008).

[4] A. Loeb, Direct measurement of cosmological parameters from the cosmic deceleration of extragalactic objects, Astrophys. J. Lett. **499**, L111 (1998).

[5] F. S. N. Lobo, J. P. Mimoso, and M. Visser, Cosmographic analysis of redshift drift, J. Cosmol. Astropart. Phys. 04 (2020) 043.

[6] A. Heinesen, Redshift drift as a model independent probe of dark energy, Phys. Rev. D **103**, L081302 (2021).

[7] S. M. Koksbang, Another look at redshift drift and the backreaction conjecture, J. Cosmol. Astropart. Phys. 10 (2019) 036.

[8] A. Heinesen, Multipole decomposition of redshift drift—Model independent mapping of the expansion history of the Universe, Phys. Rev. D **103**, 023537 (2021).

[9] S. M. Koksbang, Searching for Signals of Inhomogeneity Using Multiple Probes of the Cosmic Expansion Rate H(z), Phys. Rev. Lett. **126**, 231101 (2021).

[10] J.-P. Uzan, C. Clarkson, and G. F. R. Ellis, Time Drift of Cosmological Redshifts as a Test of the Copernican Principle, Phys. Rev. Lett. **100**, 191303 (2008).

[11] C.-M. Yoo, T. Kai, and K.-i. Nakao, Redshift drift in Lemaître-Tolman-Bondi void universes, Phys. Rev. D **83**, 043527 (2011).

[12] P. Mishra, M.-N. Celerier, and T. P. Singh, Redshift drift as a test for discriminating between different cosmological models, Phys. Rev. D **86**, 083520 (2012).

[13] A. Balcerzak and M. P. Dąbrowski, Redshift drift in a pressure gradient cosmology, Phys. Rev. D **87**, 063506 (2013).

[14] P. Fleury, C. Pitrou, and J.-P. Uzan, Light propagation in a homogeneous and anisotropic universe, Phys. Rev. D **91**, 043511 (2015).

[15] S. M. Koksbang, Observations in statistically homogeneous, locally inhomogeneous cosmological toy-models without FLRW backgrounds, Mon. Not. R. Astron. Soc. **498**, L135 (2020); **500**, L11(E) (2020).

[16] S. M. Koksbang and S. Hannestad, Redshift drift in an inhomogeneous universe: Averaging and the backreaction conjecture, J. Cosmol. Astropart. Phys. 01 (2016) 009.

[17] P. Mishra, Redshift and redshift drift in $\Lambda = 0$ quasispherical Szekeres cosmological models and the effect of averaging, Phys. Rev. D **105**, 063520 (2022).

[18] A. Balcerzak, Redshift drift and inhomogeneities, AIP Conf. Proc. **1514**, 128 (2013).

[19] M. Korzyński and J. Kopiński, Optical drift effects in general relativity, J. Cosmol. Astropart. Phys. 03 (2018) 012.

[20] M. Grasso and E. Villa, BiGONLight: Light propagation with bilocal operators in numerical relativity, Classical Quantum Gravity **39**, 015011 (2022).

[21] M. Grasso, E. Villa, M. Korzyński, and S. Matarrese, Isolating nonlinearities of light propagation in inhomogeneous cosmologies, Phys. Rev. D **104**, 043508 (2021).

[22] A. Heinesen, Redshift drift cosmography for model-independent cosmological inference, Phys. Rev. D **104**, 123527 (2021).

[23] A. J. M. Spencer, A note on the decomposition of tensors into traceless symmetric tensors, Int. J. Eng. Sci. **8**, 475 (1970).

[24] A. Heinesen, Multipole decomposition of the general luminosity distance 'Hubble law'—A new framework for observational cosmology, J. Cosmol. Astropart. Phys. 05 (2021) 008.

[25] G. Lemaître, The expanding universe, Gen. Relativ. Gravit. **29**, 641 (1997).

[26] R. C. Tolman, Effect of inhomogeneity on cosmological models, Proc. Natl. Acad. Sci. U.S.A. **20**, 169 (1934).

[27] H. Bondi, Spherically symmetrical models in general relativity, Mon. Not. R. Astron. Soc. **107**, 410 (1947).

[28] K. Bolejko, A. Krasinski, C. Hellaby, and M.-N. Célérier, *Structures in the Universe by Exact Methods: Formation, Evolution, Interactions*, Cambridge Monographs on Mathematical Physics (Cambridge University Press, Cambridge, England, 2009).

[29] J. Plebanski and A. Krasinski, *An Introduction to General Relativity and Cosmology* (Cambridge University Press, Cambridge, England, 2006).

[30] V. Marra and A. Notari, Observational constraints on inhomogeneous cosmological models without dark energy, Classical Quantum Gravity **28**, 164004 (2011).

[31] K. Van Acoleyen, LTB solutions in Newtonian gauge: From strong to weak fields, J. Cosmol. Astropart. Phys. 10 (2008) 028.

[32] M. Redlich, K. Bolejko, S. Meyer, G. F. Lewis, and M. Bartelmann, Probing spatial homogeneity with LTB models: A detailed discussion, Astron. Astrophys. **570**, A63 (2014).

[33] A. Krasinski and K. Bolejko, Redshift propagation equations in the $\beta' \neq 0$ Szekeres models, Phys. Rev. D **83**, 083503 (2011).

[34] S. M. Koksbang, Light propagation in Swiss cheese models of random close-packed Szekeres structures: Effects of anisotropy and comparisons with perturbative results, Phys. Rev. D **95**, 063532 (2017).